AMERICAN SOCIETY of
GENE & CELL
THERAPY

Reversal of Vocal Fold Mucosal Fibrosis Using siRNA against the Collagen-Specific Chaperone *Serpinh1*

Yo Kishimoto,[1,3] Masaru Yamashita,[1,4] Alice Wei,[1] Yutaka Toya,[1,5] Shuyun Ye,[2,6] Christina Kendziorski,[2] and Nathan V. Welham[1]

[1]Division of Otolaryngology, Department of Surgery, University of Wisconsin School of Medicine and Public Health, Madison, WI 53792, USA; [2]Department of Biostatistics and Medical Informatics, University of Wisconsin School of Medicine and Public Health, Madison, WI 53706, USA

Vocal fold (VF) mucosal fibrosis results in substantial voice impairment and is recalcitrant to current treatments. To reverse this chronic disorder, anti-fibrotic therapies should target the molecular pathology of aberrant collagen accumulation in the extracellular matrix. We investigated the therapeutic potential of siRNA against *Serpinh1*, a collagen-specific chaperone that enables cotranslational folding and assembly of procollagens in the endoplasmic reticulum. We implemented a previously validated siRNA construct, conducted transfection experiments using *in vitro* and *in vivo* rat models, and measured knockdown efficiency, dose responses, delivery strategies, and therapeutic outcomes. Liposome-mediated delivery of *Serpinh1*-siRNA downregulated collagen production in naive and scar VF fibroblasts as well as naive VF mucosa; moreover, sustained *Serpinh1* knockdown in fibrotic VF mucosa reversed scar-associated collagen accumulation within 4 weeks. Analysis of therapeutic effects at the transcriptome level showed evidence of cell cycle upregulation, catabolism, matrix disassembly, and morphogenesis. These findings indicate that *Serpinh1*-siRNA holds potential as a molecular therapy for chronic VF mucosal fibrosis.

INTRODUCTION

Vocal fold (VF) mucosal fibrosis can cause an intractable dysphonia that leads to substantial communication difficulty, occupational disadvantage, and social isolation.[1–4] The primary driver of this fibrosis is the VF fibroblast (VFF). Quiescent VFFs regulate extracellular matrix (ECM) turnover, helping to maintain the VF *lamina propria's* biomechanical capacity for voice production;[5] however, when activated by sustained inflammatory and profibrotic stimuli, VFFs differentiate into pathologic myofibroblasts.[6–9] These fibrogenic and contractile cells produce an abundance of disorganized fibrous proteins, most notably collagen, that negatively affect tissue viscoelasticity, biomechanics, and physiologic function.[10–13] Effective treatment of this ECM impairment is challenging. Current approaches include scar excision, biomaterial injection or implantation, steroid injection, and laser irradiation;[14–20] candidate therapies, under investigation in early-phase clinical trials, include basic fibroblast growth factor,[21] hepatocyte growth factor,[22] and autologous cells isolated from the adipose tissue-derived stromal vascular fraction.[23] Although beneficial in select cases, surgical manipulation carries a risk of further iatrogenic injury, whereas current and emerging pharmacologic, biologic, and cell therapies fail to specifically target the molecular pathology of the disordered ECM and its hallmark feature of aberrant collagen accumulation. Consequently, no treatment is uniformly effective.[14,24,25]

Mature collagen synthesis requires cotranslational folding and assembly of hydroxylated and glycosylated procollagen chains within the endoplasmic reticulum (ER). Serpin peptidase inhibitor clade H, member 1 (SERPINH1, also known as collagen-binding protein 1 [colligin], glycoprotein 46 [gp46], and heat shock protein 47 [HSP47]) is a collagen-specific chaperone protein that associates with procollagen in the ER, facilitates folding and triple helix formation, and dissociates by the time the procollagen reaches the *cis*-Golgi.[26–28] SERPINH1 synthesis is tightly aligned with that of collagen in normal and fibrotic tissues.[29–31] *Serpinh1*$^{-/-}$ mice (lethal by embryonic day 11.5 [E11.5]) and fibroblasts produce misfolded, fragile collagen helices that are easily digested;[32] further, targeted interruption of *Serpinh1* expression has been shown to reverse pathologic collagen accumulation and improve organ function in multiple *in vivo* fibrosis models.[33–36] These mechanistic and preclinical data suggest that SERPINH1 is a promising molecular target for ameliorating fibrosis and its associated morbidity.
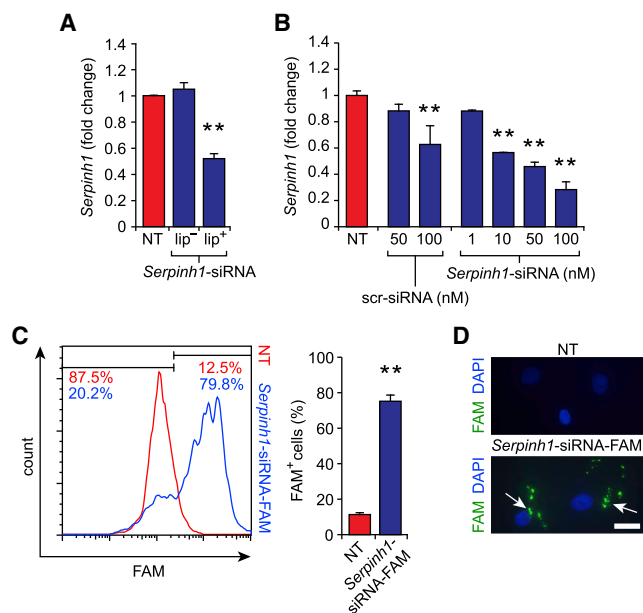
Figure 1. Liposome-Mediated Delivery of *Serpinh1*-siRNA Causes Dose-Dependent Knockdown of *Serpinh1* Transcription in VFFs

(A) Effect of *Serpinh1*-siRNA transfection on *Serpinh1* expression in naive VFFs when delivered as a naked construct (lip⁻) or via a liposomal vector (lip⁺). (B) Dose-dependent responses to *Serpinh1*-siRNA and scr-siRNA transfection in naive VFFs. (C) Uptake of 6-carboxyfluorescein-labeled siRNA (*Serpinh1*-siRNA-FAM) by VFFs. The histograms are representative; the bar chart summarizes data from both naive and scar VFFs. (D) Representative intracellular distribution of *Serpinh1*-siRNA-FAM (white arrows) in VFFs. Comparable images were obtained from naive and scar VFFs. Scale bar, 30 μm. Quantitative data are presented as mean ± SEM; n = 3–10 biological replicates per condition; **p < 0.01 versus non-transfected (NT) control. The siRNA dose was 50 nM in (A), (C), and (D). Cells for qRT-PCR were harvested 24 h following transfection. Flow cytometry and microscopy were performed immediately following transfection.

Here we investigated the feasibility and therapeutic potential of small interfering RNA (siRNA)-based *Serpinh1* interruption for treating chronic VF mucosal fibrosis. We implemented a previously validated siRNA construct,[33–36] conducted transfection experiments using robust *in vitro* and *in vivo* rat models,[6,37,38] and measured knockdown efficiency, dose responses, delivery strategies, and therapeutic outcomes. Additionally, we surveyed the transcriptomic response to *Serpinh1* interruption to identify new downstream gene targets and develop a more complete understanding of this siRNA's mechanism of action as an anti-fibrotic therapy.

RESULTS

Liposome-Mediated Delivery of *Serpinh1*-siRNA Causes Dose-Dependent Knockdown of *Serpinh1* Transcription in VFFs

Prior work has shown successful siRNA uptake by human VFFs when supported by lipofection.[39] To determine whether rat VFFs are amenable to transfection with siRNA targeting *Serpinh1*, we incubated naive cells with 50 nM *Serpinh1*-siRNA for 24 h with and without a liposomal vector. *Serpinh1*-siRNA significantly downregu-

lated *Serpinh1* expression when delivered in a liposome but had no effect when delivered as a naked construct (Figure 1A). We therefore used a liposome vector for subsequent experiments. *Serpinh1*-siRNA exhibited dose-dependent inhibition of *Serpinh1* expression in the 1- to 100-nM range, with ∼70% knockdown at 100 nM; however, delivery of negative control siRNA containing a scramble sequence (scr-siRNA) resulted in nonspecific inhibition at this dose (Figure 1B). We therefore used a 50-nM dose (for which there was no effect of scr-siRNA on *Serpinh1* expression) for subsequent *in vitro* experiments. Next we labeled *Serpinh1*-siRNA-liposome complexes with the fluorescent dye 6-carboxyfluorescein (FAM) and assessed transfection efficiency in both naive VFFs and early-passage scar VFFs that exhibit a myofibroblast phenotype.[6] After a 1-h incubation period, flow cytometry revealed signal uptake by more than 75% of cells (Figure 1C), and fluorescence microscopy confirmed intracellular (with some perinuclear) distribution (Figure 1D).

Serpinh1 Knockdown Suppresses Collagen Synthesis but Not *Col1a1* Expression in Naive and Scar VFFs

Next, to assess the effect of on *Serpinh1* inhibition on collagen production in naive and scar VFFs, we transfected cells with 50 nM *Serpinh1* siRNA and assayed gene transcription at 24 h and protein secretion at 48 h. Mature collagen secretion was inferred from hydroxyproline abundance in the culture supernatant.[40] In both naive and scar VFFs, *Serpinh1* knockdown (Figure 2A) corresponded to reduced hydroxyproline abundance (Figure 2B) but had no effect on *Col1a1* expression (Figure 2C), consistent with the proposed mechanism of SERPINH1 as a molecular chaperone that interacts with procollagen cotranslationally.[26]

Serpinh1-siRNA Causes Transient *Serpinh1* Knockdown and Reduced Collagen Abundance in Naive VF Mucosa

Given the collagen suppression effect of *Serpinh1*-siRNA in both naive and scar VFF models *in vitro*, we explored parameters for local delivery of siRNA to the bilateral VF mucosae *in vivo*. We used a rat model with transoral laryngeal exposure because the rat is a well-established preclinical model in VF scar biology[11,37,38] and because transoral exposure is minimally invasive and directly translatable to human patients.[41] First, we injected a 5-μL bolus containing 50 ng *Serpinh1*-siRNA, 50 ng scr-siRNA, or PBS to each medial VF mucosa. Injection of PBS or scr-siRNA upregulated *Serpinh1* expression at 48 h, whereas *Serpinh1*-siRNA had no effect compared with naive tissue control (Figure 3A). We reasoned that this increase in *Serpinh1* expression under both negative control conditions might be caused by an acute wound response to the injection needle and that such wound-induced transcription was neutralized by *Serpinh1*-siRNA. We therefore adjusted our technique and performed a lateral injection of 50 ng *Serpinh1*-siRNA or scr-siRNA to each posterior ventricular fold, avoiding direct injury of the VF mucosa while allowing diffusion of liposome-siRNA complexes to the target region.[42] Lateral injection of *Serpinh1*-siRNA downregulated *Serpinh1* in the VF mucosa by ∼40%, whereas scr-siRNA had no effect (Figure 3A). We therefore used a lateral injection technique for subsequent *in vivo* experiments.
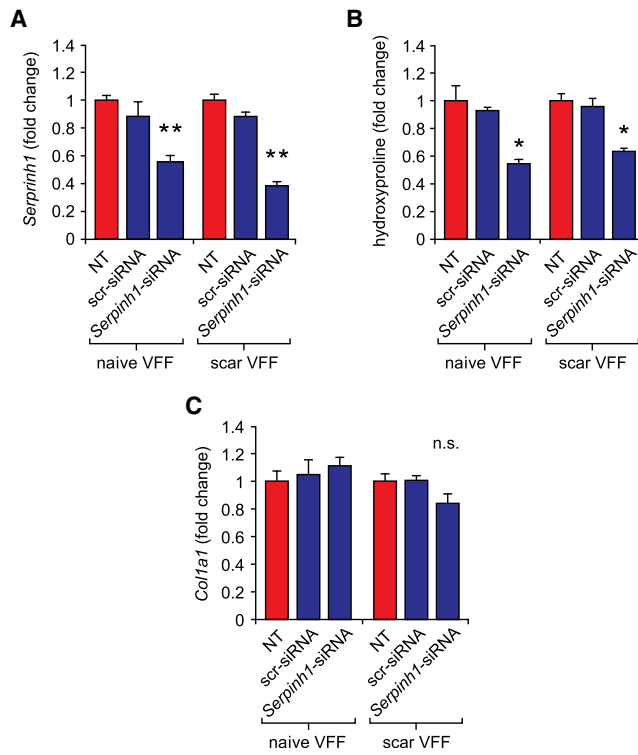
A

B

C

Figure 2. *Serpinh1* Knockdown Suppresses Collagen Synthesis but Not *Col1a1* Transcription in Naive and Scar VFFs

(A–C) Effect of *Serpinh1*-siRNA and scr-siRNA transfection on (A) *Serpinh1* expression, (B) secreted hydroxyproline abundance, and (C) *Col1a1* expression in naive and scar VFFs. Data are presented as mean ± SEM; n = 3–4 biological replicates per condition; **p < 0.01 versus NT control; *p < 0.05 versus NT control; n.s., non-significant versus NT control. The siRNA dose was 50 nM; cells for qRT-PCR were harvested 24 h following transfection. Cells for hydroxyproline analysis were collected 48 h following transfection.

We conducted additional experiments to determine the optimal dose and frequency of *Serpinh1*-siRNA delivery to achieve sustained *Serpinh1* knockdown. *Serpinh1*-siRNA doses ranging from 50–200 ng had a comparable inhibitory effect on *Serpinh1* expression at 48 h (Figure 3B); we therefore used a 50-ng dose for subsequent *in vivo* work. At the 50-ng dose, *Serpinh1* expression was most depressed at 48 h and recovered to basal levels by 6 days (Figure 3C). Parallel analysis of hydroxyproline abundance showed no effect at 48 h, followed by significant inhibition at 4 and 6 days (Figure 3D). These data highlight a delay between *Serpinh1* knockdown and its downstream effect on collagen synthesis *in vivo* and, additionally, suggest that sustained *Serpinh1* knockdown in VF mucosae requires *Serpinh1*-siRNA delivery every 3–4 days.

Sustained *Serpinh1* Knockdown Reverses Scar-Associated Collagen Accumulation in VF Mucosae

Based on these findings in naive tissue, we attempted sustained *Serpinh1* knockdown in scarred VF mucosae via serial *Serpinh1*-siRNA delivery and assessed its effect on collagen abundance and

tissue architecture. First, we performed bilateral VF mucosal injuries in rats and waited 8 weeks for scar maturation (Figure 4A).[37] We then delivered 50 ng *Serpinh1*-siRNA or scr-siRNA to each mucosa twice per week for 4 weeks; naive and untreated (scarred) VF mucosae served as additional controls. The 4-week treatment period was based on demonstrated efficacy of the same siRNA construct in multiple rat models of liver cirrhosis.[33] *Serpinh1*-siRNA treatment resulted in a significant reduction in hydroxyproline abundance compared with scr-siRNA-treated and untreated mucosae; we observed no difference between *Serpinh1*-siRNA-treated and naive mucosae (Figure 4B). Similar data were obtained for *Col1a1* expression (Figure 4C), suggesting that, unlike in the *in vitro* system (Figure 2C), cotranslational collagen suppression via *Serpinh1* interruption additionally resets transcriptional activity *in vivo*. Histological assessment revealed improved VF mucosal morphology following *Serpinh1*-siRNA treatment, characterized by less muscle fiber invasion of the *lamina propria* and reduced buckling of the epithelial contour (Figure 4D). Masson's trichrome staining as well as COL1 and COL3 immunostaining corroborated the hydroxyproline data (Figures 4D–4F) and confirmed that sustained *Serpinh1* knockdown reverses scar-associated collagen accumulation in VF mucosae.

Serpinh1 Knockdown Induces a Transcriptome-Level Shift in Cell Phenotype

Given that *Serpinh1*-siRNA reversed the histologic and collagen deposition features of VF mucosal fibrosis, a multifaceted ECM disorder, we questioned whether *Serpinh1* knockdown affects additional downstream targets beyond collagen. Existing data indicate that this siRNA does not induce an interferon-α-mediated immune response or other off-target effects;[33] in addition to its targeted effect on *de novo* collagen assembly, its therapeutic mechanism is hypothesized to include sustained activity by matrix mellatoproteinase (MMP) enzymes and apoptosis of collagen-synthesizing cells.[33,34,36,43] To identify additional gene sets and pathways that are downstream of *Serpinh1* interruption, we returned to the *in vitro* model, used expression microarrays to profile the transcriptomes of *Serpinh1*-siRNA- and scr-siRNA-treated scar VFFs, and compared these with previously reported data from naive and untreated scar VFFs.[6] We used an empirical Bayes approach to evaluate equivalent and differential gene expression (equivalent expression [EE] and differential expression [DE], respectively)[44] and built two statistical models to identify therapeutically relevant gene sets of interest. First, using three-way comparisons, we identified genes with an expression pattern indicative of an siRNA-induced therapeutic shift from the scar VFF phenotype: DE between *Serpinh1*-siRNA and both scr-siRNA and untreated scar VFF conditions as well as EE between scr-siRNA and untreated scar VFF conditions (Figure 5A). A total of 551 oligonucleotide probes corresponding to 388 unique genes fit this expression pattern. Enrichment analysis of this gene set, conducted using Enrichr[45,46] and Gene Ontology annotations,[47] highlighted clusters of biological process terms associated with mitosis and cell division, metabolism and catabolism, ECM disassembly, development and morphogenesis, and a non-specific stimulus response; cellular component terms primarily associated with the
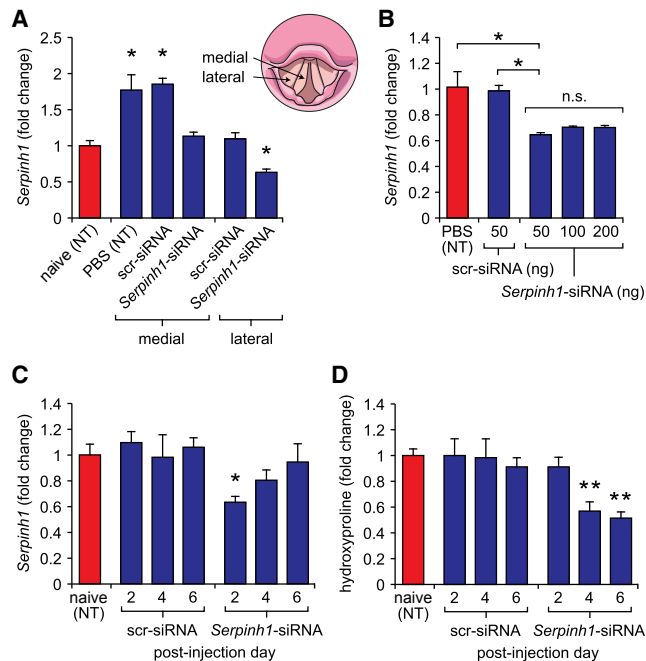
Figure 3. Effect of *Serpinh1*-siRNA Delivery to Naive VF Mucosae

(A) Comparison of *Serpinh1* expression following medial or lateral injection of *Serpinh1*-siRNA, scr-siRNA, or PBS to naive rat VF mucosae. The schematic illustrates needle placement; all injections were performed bilaterally. (B) Effect of *Serpinh1*-siRNA dose escalation on *Serpinh1* expression. (C) Time course of *Serpinh1* expression following *Serpinh1*-siRNA or scr-siRNA transfection. (D) Time course of hydroxyproline abundance following *Serpinh1*-siRNA or scr-siRNA transfection. Data are presented as mean ± SEM; n = 3–6 biological replicates per condition; **p < 0.01 versus naive (NT) control; *p < 0.05 versus naive (NT) control or as otherwise indicated in (B). The siRNA dose was 50 ng in (A), (C), and (D). A lateral injection site was used in (B)–(D). Cells for qRT-PCR were harvested 48 h following transfection in (A) and (B).

nucleus and ECM; and molecular function terms associated with ATP and microtubule binding as well as DNA binding and transcriptional regulation.

Next, using four-way comparisons that included the naive VFF condition, we identified genes with an expression pattern indicative of therapeutic normalization, defined as a shift from the scar VFF to naive VFF phenotype: EE between *Serpinh1*-siRNA and naive VFF conditions and between scr-siRNA and untreated scar VFF conditions; DE for comparisons between all other conditions (Figure 5B). These criteria yielded 39 probes associated with 33 unique genes. Fourteen of these genes were upregulated in the *Serpinh1*-siRNA and naive VFF conditions, including the cell cycle-regulatory genes *Ccna2*, *Mki67*, and *S100b* as well as the mesoderm differentiation and pattern formation gene *Tbx4*. The remaining 19 genes were downregulated, including the ECM-related genes *Acan*, *Tnn*, and *Tgfbi*; the immunoregulatory genes *C3*, *C1qtnf3*, and *Ccl11*; and the cytoskeleton-associated genes *Acta1*, *Actg2*, *Cnn1*, *Epb41l4a*, *Myh11*, *Myh2*, and *Sgcg*. Enrichment analysis of the entire gene set identified cellular component terms associated with the extracellular

region; we identified no enrichment of terms in the biological process or molecular function domains.

DISCUSSION

VF mucosal fibrosis is associated with substantial morbidity;[1–4] however, to date, most preclinical treatment research has focused on scar prophylaxis via manipulation of early wound healing events.[48–52] Here, we directly tackled the molecular pathology of chronic VF mucosal fibrosis by targeting collagen assembly and accumulation in the disordered ECM. Liposome-mediated delivery of siRNA against the collagen-specific chaperone *Serpinh1* downregulated collagen production in naive and scar VFFs as well as naive rat VF mucosae; further, sustained *Serpinh1* knockdown in rat VF mucosae reversed scar-associated collagen accumulation within a 4-week period. These findings show that *Serpinh1*-siRNA holds potential as a molecular therapy for chronic VF mucosal fibrosis.

Prior work suggests that interruption of *Serpinh1* expression ameliorates fibrosis through several mechanisms. Misfolded procollagen molecules accumulate in the ER of transfected cells, overwhelm their autophagy machinery, and drive stress-mediated apoptosis.[43] A repository of ECM-associated MMPs remains available to digest pre-existing (stable) and any newly synthesized (fragile) collagen, which may drive further apoptosis by anoikis.[33,34,36] Of note, this apoptosis of collagen-producing cells may indirectly account for the reduction in *Col1a1* transcription observed in our *in vivo* data; a similar effect was reported following *Serpinh1*-siRNA treatment of cirrhotic liver.[33] Our transcriptomic data corroborated these suggested mechanisms by identifying *Serpinh1*-siRNA-induced expression patterns indicative of ECM disassembly, catabolism, and cell cycle regulation, for which many regulatory genes and components of the nuclear machinery play a role in both apoptosis and proliferation.[53] We further discovered DE genes and gene sets associated with immunoregulation as well as morphogenesis and pattern formation, indicating that *Serpinh1* interruption may achieve its therapeutic effect via multiple downstream pathways and regenerative functions.

siRNA transfection is inherently vulnerable to off-target effects and stimulation of innate immune responses, making careful oligonucleotide design and the inclusion of suitable controls imperative to appropriate data interpretation. We utilized a previously validated *Serpinh1*-siRNA construct[33] comprised of a 27-nt RNA duplex (designed to optimize potency)[54] containing a 2-nt 3′ overhang and no 5′ triphosphate terminus (designed to mitigate interferon induction).[55] Our scr-siRNA data confirmed the absence of nonspecific effects at therapeutic doses during *in vitro* and *in vivo* experiments; a prior report, focused on hepatic stellate cells and cirrhotic liver, validated the specificity of the *Serpinh1*-siRNA construct and absence of a bystander effect by showing equivalent knockdown and reversal of fibrosis with two other siRNAs against the same mRNA target.[33] This prior work additionally showed no evidence of a *Serpinh1*-siRNA-triggered innate immune response *in vivo*. Despite these encouraging findings, future preclinical studies should carefully assess
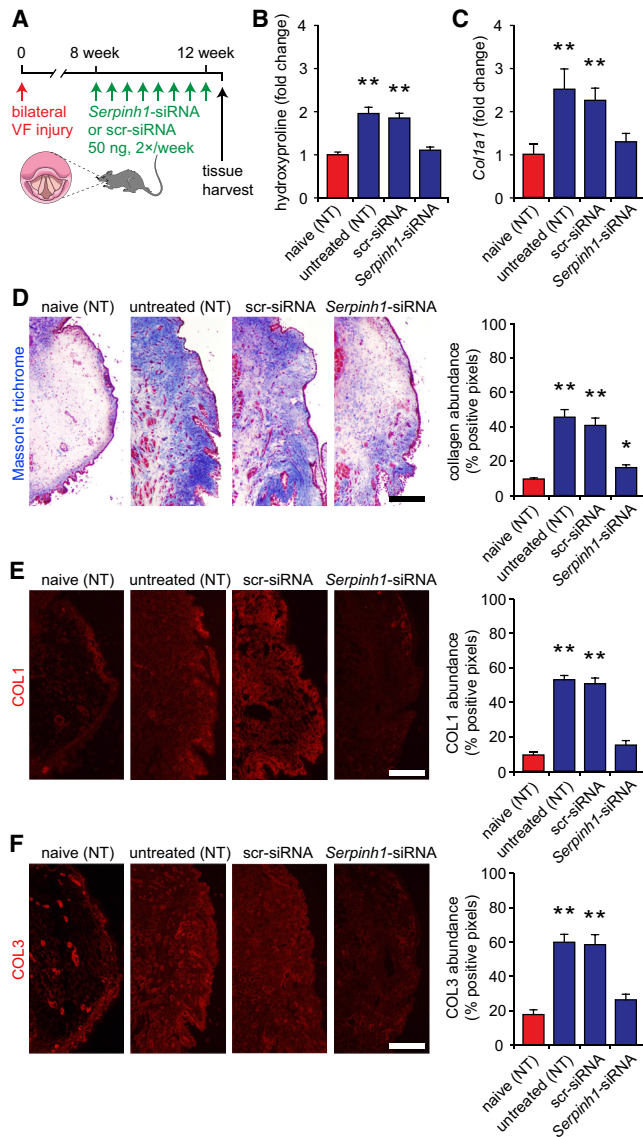
Figure 4. Sustained *Serpinh1* Knockdown Reverses Scar-Associated Collagen Accumulation in VF Mucosae

(A) Schematic illustrating the injury, scar formation, and siRNA delivery schedule. Tissue harvest occurred 4 days following the final siRNA dose. (B) Hydroxyproline abundance. (C) *Col1a1* expression. (D) Representative Masson's trichrome-stained coronal VF sections and corresponding analysis of total collagen abundance. (E) Representative COL1-immunostained coronal VF sections and corresponding analysis of COL1 abundance. (F) Representative COL3-immunostained coronal VF sections and corresponding analysis of COL3 abundance. Quantitative data are presented as mean ± SEM; n = 5 biological replicates per condition; **p < 0.01 versus naive (NT) control; *p < 0.05 versus naive (NT) control. A lateral injection site was used. Image analysis data represent the *lamina propria* region. Scale bars, 200 μm (D–F).

off-target or other adverse effects of local *Serpinh1*-siRNA delivery to the larynx. In addition, because age and sex influence VF biology[56–59] (and our data were generated using 4- to 7-month-old male rats),

future studies should evaluate the effect of these biological variables on *Serpinh1* knockdown and therapeutic response.

With a view to clinical translation, we used transoral injection to non-traumatically deliver *Serpinh1*-siRNA to the VF mucosae via diffusion and further identified the optimal dose and delivery frequency required for sustained *Serpinh1* knockdown *in vivo*. Other work targeting *Serpinh1* has used vitamin A-conjugated liposomes to traffic *Serpinh1*-siRNA to hepatic and pancreatic stellate cells[33,36] as well as lung and skin myofibroblasts.[34,35] Such an approach harnesses physiologic transport via plasma retinol-binding protein to facilitate intravenous delivery to target cells. We did not explore this approach in the current study because, unlike in other organs, vitamin A-storing VF stellate cells are clustered in distinct anatomic niches[60] and do not appear to be the primary cells responsible for fibrosis.[38,61,62] Further improvement in *Serpinh1*-siRNA delivery to fibroblasts throughout the VF mucosae might be achieved with a controlled-release system,[63] increasing the duration of *Serpinh1* knockdown and, as a result, the interval between injections.

MATERIALS AND METHODS

Animals

Fischer 344 inbred male rats (Charles River Laboratories) were used for all experiments; all procedures were approved by the Animal Care and Use Committee of the University of Wisconsin School of Medicine and Public Health. Four-month-old rats received bilateral VF mucosal injuries as described previously,[37,38] followed by a 2-month scar maturation period. These rats were then used for scar VFF isolation and primary culture or reserved for *in vivo* siRNA experiments. Uninjured age-matched rats were used for naive VFF isolation and primary culture (6 months old) and as naive controls in the *in vivo* siRNA experiments (7 months old).

Primary Cell Isolation and Culture

Primary VFF cultures were conducted using an explant culture technique.[6] Briefly, bilateral VF mucosae were microdissected from freshly harvested rat larynges, minced in a 10-cm culture dish, and immersed in DMEM supplemented with 10% fetal bovine serum (FBS), L-glutamine, antibiotics, and antimycotics (all reagents from Sigma-Aldrich). Cells were cultured at 37°C in 5% CO_2; medium was exchanged twice per week. Outgrown primary cells were trypsinized and passaged 14–21 days after initial explant plating.

siRNA Preparation

We used previously reported 27-nt RNA duplexes with 2-nt 3′ overhangs (Hokkaido System Science) designed to maximize silencing efficacy and minimize immune activation.[33] The sense and anti-sense strands were as follows: *Serpinh1*, beginning at nucleotide 757, 5′-GUUCCACCAUAAGAUGGUAGACAACAG-3′ (sense), 5′-GUUG UCUACCAUCUUAUGGUGGAACAU-3′ (antisense); scramble, 5′-CGAUUCGCUAGACCGGCUUCAUUGCAG-3′ (sense), 5′-GCAAUG AAGCCGGUCUAGCGAAUCGAU-3′ (antisense). In experiments designed to confirm siRNA uptake via flow cytometry and
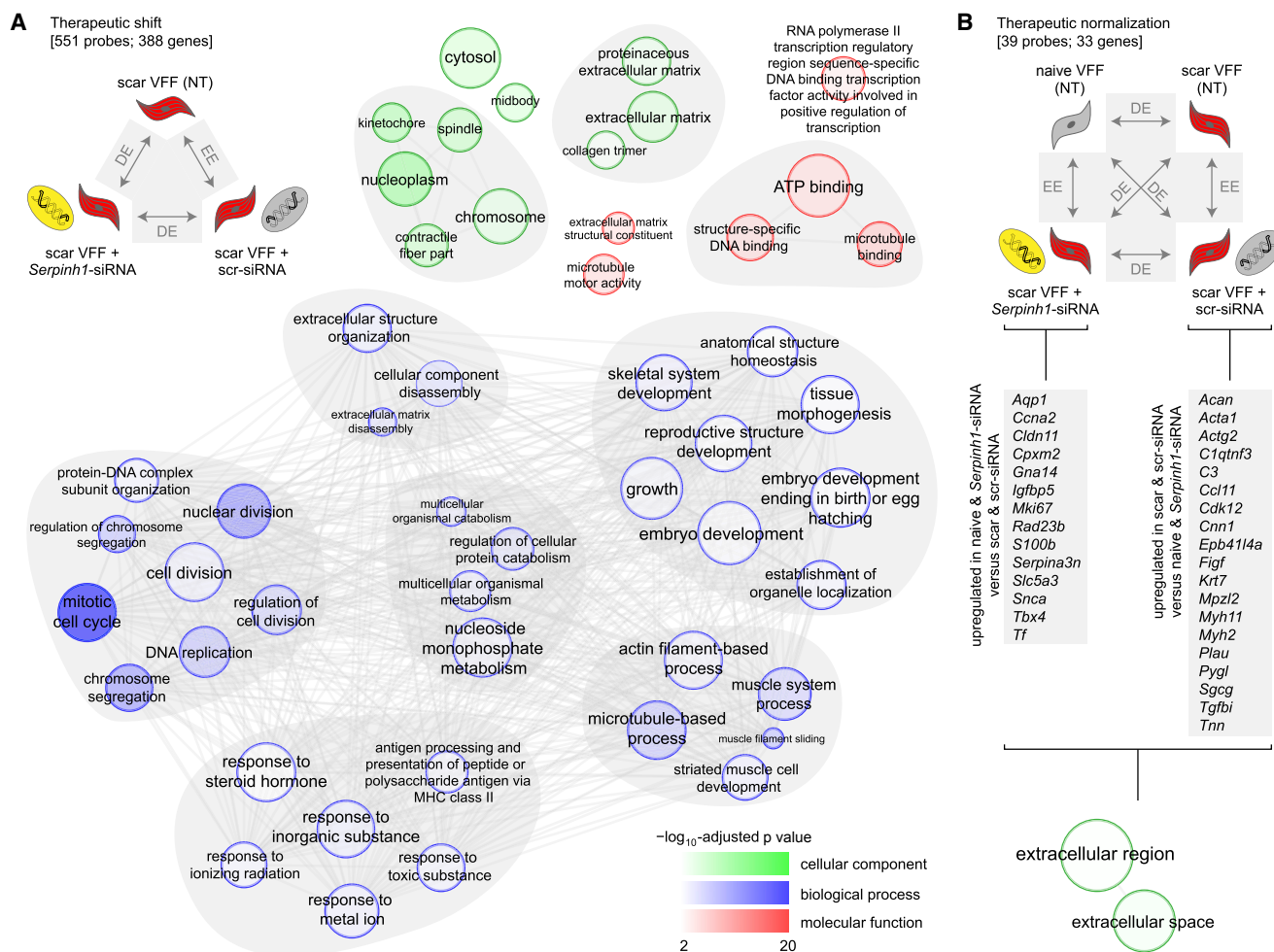
Figure 5. *Serpinh1* Knockdown Induces a Transcriptome-Level Shift in Cell Phenotype

(A) Analysis of *Serpinh1*-induced therapeutic shift in the scar VFF transcriptome. The experimental schematic (top left) represents the three-way expression pattern of interest, defined as a therapeutic shift from the scar VFF phenotype. EE, equivalent expression; DE, differential expression. The remainder summarizes the enrichment analysis of 388 genes that fit this therapeutic shift pattern. Enriched Gene Ontology terms are depicted as nodes; node and label font size are proportional to the generality of the term in the underlying ontology. Cellular component terms are shown in green; molecular function terms are shown in red; biological process terms are shown in blue. Node color intensity represents the $-\log_{10}$-adjusted p value associated with term enrichment. Nodes representing semantically similar terms are connected by gray lines and grouped within gray ovals. (B) Analysis of *Serpinh1*-induced therapeutic normalization in the scar VFF transcriptome. The experimental (top) schematic represents the four-way expression pattern of interest, defined as a shift from the scar VFF to naive VFF phenotype. The 33 genes that fit this therapeutic normalization pattern are listed according to upregulation (n = 14) or downregulation (n = 19) under both *Serpinh1*-siRNA and naive VFF conditions. Enrichment analysis (lower region) was performed using the entire gene set and exclusively identified terms in the cellular component domain. Analyses were performed with 3–4 biological replicates per condition. The siRNA dose was 50 nM. Cells were harvested 24 h following transfection.

fluorescence microscopy, *Serpinh1*-siRNA was prepared with FAM coupled to the 5′ end of the sense strand.

siRNA Transfection of VFFs

All *in vitro* experiments were performed at passage 1 (P1), based on data showing that the scar and naive VFF phenotypes coalesce at later passages.[6] Cells were seeded in 6-well plates or 2-well chamber slides at a density of 2×10^4 cell/well and cultured until 80% confluent. Immediately prior to transfection, the culture medium was aspirated, and cells were rinsed in PBS.

Transfection was performed using the Lipotrust delivery system (Hokkaido System Science) according to the manufacturer's protocol. Each 2-mL transfection preparation contained 1.8 mL Opti-MEM (Invitrogen) supplemented with 10% FBS and 200 μL siRNA-liposome complex comprised of 2–200 pmol siRNA (corresponding to a 1- to 100-nM final concentration) and 40 nmol cationic lipid. In one experiment, where indicated, transfection was performed without the liposomal vector. Cells were incubated with the siRNA preparation at 37°C for 1 h, rinsed in PBS, and either harvested for immediate flow cytometry and fluorescence microscopy or maintained in culture for a further 24 or 48 h.

siRNA Delivery to Rat VF Mucosae

Rats were anesthetized using an intraperitoneal cocktail of 90 mg/kg ketamine hydrochloride and 9 mg/kg xylazine hydrochloride; 0.05 mg/kg atropine sulfate was used to reduce secretions in the laryngeal lumen. The larynx was visualized via a 1.9-mm diameter, 25° rigid endoscope (Richard Wolf), and 5 μL siRNA-liposome complex (containing 50–200 ng siRNA) or PBS was injected to the medial or lateral VF mucosae bilaterally. Injections were performed using a microsyringe and 33G needle (Hamilton). Rats in the pilot experiment received one pair of bilateral injections, followed by larynx harvest at 2, 4, or 6 days; rats in the therapeutic trial received serial bilateral injections twice per week for 4 weeks. Larynges were harvested 4 days following the final injection.

RNA Isolation and qRT-PCR

Total RNA was isolated from pelleted cells and VF mucosa using the RNeasy Mini kit (QIAGEN) according to the manufacturer's protocol. Samples were treated with DNase I to eliminate contamination by genomic DNA (Ambion); protein was acetone-precipitated from the column flowthrough and reserved for hydroxyproline measurement. RNA yield and purity were evaluated with a NanoDrop ND-1000 spectrophotometer. cDNA was generated by reverse transcription using TaqMan reagents (Applied Biosystems).

qRT-PCR amplification was performed using rat-specific commercial primers (QuantiTect, QIAGEN): QT00370622 (*Col1a1*), QT00195958 (*Sdha*), and QT01081010 (*Serpinh1*). Reactions were performed on a 7500 Fast Real-Time PCR system (Applied Biosystems) using the QuantiTect SYBR Green PCR kit (QIAGEN). Each 25-μL total volume reaction contained 12.5 μL 2 × QuantiTect master mix, 2.5 μL 10 × QuantiTect primer assay, and 10 μL cDNA template diluted in nuclease-free H_2O. The cycling program was as follows: initial activation at 95°C for 15 min, followed by 40 cycles of 94°C for 15 s, 55°C for 30 s, and 72°C for 30 s. All PCR reactions were performed in technical duplicates. Relative mRNA expression was calculated using the $2^{-\Delta\Delta CT}$ method;[64] data were normalized against the reference gene *Sdha*.[65]

Microarrays

Biotinylated antisense cRNA was prepared by single-round *in vitro* amplification of 0.9 μg input RNA using the MessageAmp II-Biotin Enhanced aRNA kit (Ambion) according to the manufacturer's instructions (the *in vitro* transcription reaction was performed at 37°C for 14 h). Polyadenylated RNA controls (Affymetrix) were spiked into each reaction. Fragmented cRNA sample quality was confirmed using 2% agarose gel electrophoresis and Agilent 2100 Bioanalyzer analysis. Samples were hybridized to Affymetrix GeneChip Rat Genome 230 2.0 arrays at 45°C for 16 h. Post-processing was performing using the GeneChip Fluidics Station 450, arrays were scanned using the GC3000 G7 scanner, and fluorescent intensity data were background-corrected and extracted using Expression Console software (Affymetrix). All hybridization, post-processing, and scanning procedures were performed according to Affymetrix protocols; all control parameters were within the manufacturer's guidelines. Microarray data are available from the Gene Expression Omnibus (GEO): GSE62204 (https://www.ncbi.nlm.nih.gov/geo/).

Flow Cytometry

Serpinh1-siRNA-FAM-treated and naive VFFs were harvested, washed, pelleted, and resuspended in PBS containing 1% BSA. Flow cytometry was performing using a FACSCalibur instrument (BD Biosciences); data were analyzed in FlowJo 8.7.1 (Tree Star).

Hydroxyproline Assay

Hydroxyproline concentration in culture supernatant (100 μL) and VF mucosae (10 μg tissue-isolated protein) was assayed using the Hydroxyproline Colorimetric Assay kit (BioVision) according to the manufacturer's protocol. Acid hydrolysis was performed for 3 h at 120°C. Absorbance was measured at 560 nm using a FlexStation 3 microplate reader (Molecular Devices).

Cytochemistry, Histology, and Immunohistochemistry

Serpinh1-siRNA-FAM-treated and naive VFFs, cultured on chamber slides, were fixed using 4% paraformaldehyde (PFA) and counterstained with DAPI (MP Biomedicals) for 20 min prior to imaging.

Explanted larynges were dehydrated in PBS containing 25% sucrose at 4°C for 24 h, embedded in optimal cutting temperature compound (Tissue-Tek), and snap-frozen using acetone and dry ice. Serial 8-μm coronal sections were prepared using a cryostat (CM-3050 S, Leica Microsystems), air-dried, and stored at –80°C prior to staining.

Masson's trichrome staining was performed using a commercial kit (Newcomer Supply) according to the manufacturer's protocol. Sections intended for immunostaining were fixed with 4% PFA for 4 min and permeabilized with 0.5% Triton X-100 (Sigma-Aldrich) for 15 min. Image-iT FX signal enhancer (Invitrogen) was applied for 30 min, followed by blocking with Block Ace (AbD Serotec) for 10 min. Sections were sequentially incubated with a primary antibody for 1 h and a relevant secondary antibody for 1 h and counterstained with DAPI (MP Biomedicals) for 20 min. All procedures were performed at room temperature; slides were washed 3 times, 5 min per wash, between each step.

The primary antibodies used were goat anti-collagen type I (1:20; 1310-01, Southern Biotechnology) and rabbit anti-collagen type III (1:50; 600-401-105, Rockland Immunochemicals). The secondary antibodies used were Alexa Fluor 594 goat anti-rabbit or donkey anti-goat immunoglobulin G (IgG; 1:400, A-11012 or A-11058, Invitrogen). Negative controls, exposed to the secondary antibody in the absence of the primary antibody, revealed no immunostain.

Microscopy and Image Analysis

Light and fluorescence microscopy were performed using a Nikon E-600 microscope and Olympus DP-71 camera; images were captured with consistent exposure settings. For all collagen stains, MetaMorph 7.5 (Molecular Devices) was used to quantify the positively stained area within the *lamina propria* (defined as the region

between the basement membrane and thyroarytenoid muscle) of each VF coronal section. The threshold value for determining a positive signal was set according to each stain's background signal strength and corresponding negative control; this value was applied consistently across all samples. The number of positive pixels was normalized to the *lamina propria* cross-sectional area and expressed as a percentage.

Statistical Analysis

All experiments were performed with 3–10 independent biological replicates per condition; sample sizes for each experiment are reported in the corresponding figure legends. With the exception of microarray data, analyses were performed using SAS 9.2 (SAS Institute). Raw data were initially evaluated for normality and equality of variance using visual inspection of plots and Levene's test; data were rank- or log-transformed where indicated to meet assumptions for parametric testing. qRT-PCR, hydroxyproline, and histologic or immunohistologic stain density data were analyzed using one-way ANOVA; flow cytometry data were analyzed using a paired t test. In the ANOVA models, when the omnibus F test revealed a significant difference, planned pairwise comparisons were performed using Fisher's protected least significant difference method. A type I error rate of 0.05 was used; p values were two-sided.

Microarray data were analyzed within R.[66] Probe-level data were preprocessed using robust multiarray analysis,[67] based on evidence of improved precision over default Affymetrix algorithms.[68] Probes without a corresponding gene symbol were purged from all gene-level analyses. In cases where multiple probes corresponded to a single gene symbol, we calculated the average expression for each probe across arrays and selected the probe with the median average expression. In the case of an even number of matched probes, we selected the larger of the two median probe intensities. The resulting normalized data were clustered to check for consistency prior to formal analysis.

Expression analysis was performed using an empirical Bayes approach as implemented in the R package EBarrays.[44] A lognormal-normal (LNN) model was fit to the data. Parameter estimates were obtained via 20 iterations of an expectation-maximization algorithm; in all cases, convergence was achieved after 10 iterations. Diagnostic testing of the LNN assumption in EBarrays was performed using quantile-quantile (QQ) plots of log intensity data versus a standard normal distribution. We further used QQ plots to evaluate the assumption of a scaled inverse χ^2 prior on the gene-specific variances used in the LNN model. The diagnostics showed no violations of model assumptions.

Using the output from EBarrays, we compared expression levels under *Serpinh1*-siRNA and scr-siRNA conditions at P1 with previously reported microarray data from naive and scar rat VFFs at P1.[6] These previously reported data were generated in parallel to the siRNA transfection data using an identical cell isolation and culture protocol as well as identical RNA extraction, amplification, hybridization, and post-processing protocols. For all comparisons, thresholding was performed using more than 0.95 posterior probability of DE, corresponding to a 5% false discovery rate.

Tests of enrichment via overrepresentation were conducted using Enrichr,[45,46] the Gene Ontology dataset,[47] and genes that fit the expression patterns of interest. Overrepresented Gene Ontology terms required at least 10 distinct DE genes and a Benjamini-Hochberg adjusted p value of less than 0.01 and were further processed using the REViGO semantic similarity and term redundancy algorithm[69] followed by Cytoscape 2.8.2.[70]

AUTHOR CONTRIBUTIONS

Y.K. designed all experiments, conducted *in vitro* and *in vivo* experiments, analyzed data, and helped write the manuscript. M.Y. conceived the study and performed *in vitro* pilot testing. A.W. and Y.T. assisted with *in vivo* experiments and analyzed data. S.Y. analyzed all microarray data under the direction of C.K. N.V.W. helped to develop the study, obtained funding, assisted with design and implementation of *in vivo* and *in vitro* experiments, analyzed data, and helped write the manuscript. All authors reviewed and approved the final version.

CONFLICTS OF INTEREST

The authors declare no competing interests.

ACKNOWLEDGMENTS

REFERENCES

1. Welham, N.V., Dailey, S.H., Ford, C.N., and Bless, D.M. (2007). Voice handicap evaluation of patients with pathologic sulcus vocalis. Ann. Otol. Rhinol. Laryngol. *116*, 411–417.

2. Rosen, C.A., Lee, A.S., Osborne, J., Zullo, T., and Murry, T. (2004). Development and validation of the voice handicap index-10. Laryngoscope *114*, 1549–1556.

3. Cohen, S.M., Kim, J., Roy, N., Asche, C., and Courey, M. (2012). Direct health care costs of laryngeal diseases and disorders. Laryngoscope *122*, 1582–1588.

4. Cohen, S.M., Dupont, W.D., and Courey, M.S. (2006). Quality-of-life impact of non-neoplastic voice disorders: a meta-analysis. Ann. Otol. Rhinol. Laryngol. *115*, 128–134.

5. Gray, S.D. (2000). Cellular physiology of the vocal folds. Otolaryngol. Clin. North Am. *33*, 679–698.

6. Kishimoto, Y., Kishimoto, A.O., Ye, S., Kendziorski, C., and Welham, N.V. (2016). Modeling fibrosis using fibroblasts isolated from scarred rat vocal folds. Lab. Invest. *96*, 807–816.

7. Jetté, M.E., Hayer, S.D., and Thibeault, S.L. (2013). Characterization of human vocal fold fibroblasts derived from chronic scar. Laryngoscope *123*, 738–745.

8. Vyas, B., Ishikawa, K., Duflo, S., Chen, X., and Thibeault, S.L. (2010). Inhibitory effects of hepatocyte growth factor and interleukin-6 on transforming growth factor-β1 mediated vocal fold fibroblast-myofibroblast differentiation. Ann. Otol. Rhinol. Laryngol. 119, 350–357.

9. Branco, A., Bartley, S.M., King, S.N., Jetté, M.E., and Thibeault, S.L. (2016). Vocal fold myofibroblast profile of scarring. Laryngoscope 126, E110–E117.

10. Hirano, S., Minamiguchi, S., Yamashita, M., Ohno, T., Kanemaru, S., and Kitamura, M. (2009). Histologic characterization of human scarred vocal folds. J. Voice 23, 399–407.

11. Welham, N.V., Montequin, D.W., Tateya, I., Tateya, T., Choi, S.H., and Bless, D.M. (2009). A rat excised larynx model of vocal fold scar. J. Speech Lang. Hear. Res. 52, 1008–1020.

12. Rousseau, B., Hirano, S., Scheidt, T.D., Welham, N.V., Thibeault, S.L., Chan, R.W., and Bless, D.M. (2003). Characterization of vocal fold scarring in a canine model. Laryngoscope 113, 620–627.

13. Thibeault, S.L., Gray, S.D., Bless, D.M., Chan, R.W., and Ford, C.N. (2002). Histologic and rheologic characterization of vocal fold scarring. J. Voice 16, 96–104.

14. Friedrich, G., Dikkers, F.G., Arens, C., Remacle, M., Hess, M., Giovanni, A., Duflo, S., Hantzakos, A., Bachy, V., and Gugatschka, M.; European Laryngological Society. Phonosurgery Committee (2013). Vocal fold scars: current concepts and future directions. Consensus report of the Phonosurgery Committee of the European Laryngological Society. Eur. Arch. Otorhinolaryngol. 270, 2491–2507.

15. Mortensen, M.M., Woo, P., Ivey, C., Thompson, C., Carroll, L., and Altman, K. (2008). The use of the pulse dye laser in the treatment of vocal fold scar: a preliminary study. Laryngoscope 118, 1884–1888.

16. Mortensen, M., and Woo, P. (2006). Office steroid injections of the larynx. Laryngoscope 116, 1735–1739.

17. Young, W.G., Hoffman, M.R., Koszewski, I.J., Whited, C.W., Ruel, B.N., and Dailey, S.H. (2016). Voice outcomes following a single office-based steroid injection for vocal fold scar. Otolaryngol. Head Neck Surg. 155, 820–828.

18. Kishimoto, Y., Hirano, S., Kojima, T., Kanemaru, S., and Ito, J. (2009). Implantation of an atelocollagen sheet for the treatment of vocal fold scarring and sulcus vocalis. Ann. Otol. Rhinol. Laryngol. 118, 613–620.

19. Sataloff, R.T., Spiegel, J.R., Hawkshaw, M., Rosen, D.C., and Heuer, R.J. (1997). Autologous fat implantation for vocal fold scar: a preliminary report. J. Voice 11, 238–246.

20. Molteni, G., Bergamini, G., Ricci-Maccarini, A., Marchese, C., Ghidini, A., Alicandri-Ciufelli, M., Luppi, M.P., and Presutti, L. (2010). Auto-crosslinked hyaluronan gel injections in phonosurgery. Otolaryngol. Head Neck Surg. 142, 547–553.

21. Kanazawa, T., Komazawa, D., Indo, K., Akagi, Y., Lee, Y., Nakamura, K., Matsushima, K., Kunieda, C., Misawa, K., Nishino, H., and Watanabe, Y. (2015). Single injection of basic fibroblast growth factor to treat severe vocal fold lesions and vocal fold paralysis. Laryngoscope 125, E338–E344.

22. Hirano, S., Kawamoto, A., Tateya, I., Mizuta, M., Kishimoto, Y., Hiwatashi, N., Kawai, Y., Tsuji, T., Suzuki, R., Kaneko, M., et al. (2018). A phase I/II exploratory clinical trial for intracordal injection of recombinant hepatocyte growth factor for vocal fold scar and sulcus. J. Tissue Eng. Regen. Med. 12, 1031–1038.

23. Mattei, A., Magalon, J., Bertrand, B., Grimaud, F., Revis, J., Velier, M., Veran, J., Dessi, P., Sabatier, F., and Giovanni, A. (2018). Autologous adipose-derived stromal vascular fraction and scarred vocal folds: first clinical case report. Stem Cell Res. Ther. 9, 202.

24. Welham, N.V., Choi, S.H., Dailey, S.H., Ford, C.N., Jiang, J.J., and Bless, D.M. (2011). Prospective multi-arm evaluation of surgical treatments for vocal fold scar and pathologic sulcus vocalis. Laryngoscope 121, 1252–1260.

25. Dailey, S.H., and Ford, C.N. (2006). Surgical management of sulcus vocalis and vocal fold scarring. Otolaryngol. Clin. North Am. 39, 23–42.

26. Ishida, Y., and Nagata, K. (2011). Hsp47 as a collagen-specific molecular chaperone. Methods Enzymol. 499, 167–182.

27. Ono, T., Miyazaki, T., Ishida, Y., Uehata, M., and Nagata, K. (2012). Direct in vitro and in vivo evidence for interaction between Hsp47 protein and collagen triple helix. J. Biol. Chem. 287, 6810–6818.

28. Widmer, C., Gebauer, J.M., Brunstein, E., Rosenbaum, S., Zaucke, F., Drögemüller, C., Leeb, T., and Baumann, U. (2012). Molecular basis for the action of the collagen-specific chaperone Hsp47/SERPINH1 and its structure-specific client recognition. Proc. Natl. Acad. Sci. USA 109, 13243–13247.

29. Sunamoto, M., Kuze, K., Iehara, N., Takeoka, H., Nagata, K., Kita, T., and Doi, T. (1998). Expression of heat shock protein 47 is increased in remnant kidney and correlates with disease progression. Int. J. Exp. Pathol. 79, 133–140.

30. Brown, K.E., Broadhurst, K.A., Mathahs, M.M., Brunt, E.M., and Schmidt, W.N. (2005). Expression of HSP47, a collagen-specific chaperone, in normal and diseased human liver. Lab. Invest. 85, 789–797.

31. Chen, J.-J., Zhao, S., Cen, Y., Liu, X.X., Yu, R., and Wu, D.M. (2007). Effect of heat shock protein 47 on collagen accumulation in keloid fibroblast cells. Br. J. Dermatol. 156, 1188–1195.

32. Nagai, N., Hosokawa, M., Itohara, S., Adachi, E., Matsushita, T., Hosokawa, N., and Nagata, K. (2000). Embryonic lethality of molecular chaperone hsp47 knockout mice is associated with defects in collagen biosynthesis. J. Cell Biol. 150, 1499–1506.

33. Sato, Y., Murase, K., Kato, J., Kobune, M., Sato, T., Kawano, Y., Takimoto, R., Takada, K., Miyanishi, K., Matsunaga, T., et al. (2008). Resolution of liver cirrhosis using vitamin A-coupled liposomes to deliver siRNA against a collagen-specific chaperone. Nat. Biotechnol. 26, 431–442.

34. Otsuka, M., Shiratori, M., Chiba, H., Kuronuma, K., Sato, Y., Niitsu, Y., and Takahashi, H. (2017). Treatment of pulmonary fibrosis with siRNA against a collagen-specific chaperone HSP47 in vitamin A-coupled liposomes. Exp. Lung Res. 43, 271–282.

35. Yamakawa, T., Ohigashi, H., Hashimoto, D., Hayase, E., Takahashi, S., Miyazaki, M., Minomi, K., Onozawa, M., Niitsu, Y., and Teshima, T. (2018). Vitamin A-coupled liposomes containing siRNA against HSP47 ameliorate skin fibrosis in chronic graft-versus-host disease. Blood 131, 1476–1485.

36. Ishiwatari, H., Sato, Y., Murase, K., Yoneda, A., Fujita, R., Nishita, H., Birukawa, N.K., Hayashi, T., Sato, T., Miyanishi, K., et al. (2013). Treatment of pancreatic fibrosis with siRNA against a collagen-specific chaperone in vitamin A-coupled liposomes. Gut 62, 1328–1339.

37. Tateya, T., Tateya, I., Sohn, J.H., and Bless, D.M. (2005). Histologic characterization of rat vocal fold scarring. Ann. Otol. Rhinol. Laryngol. 114, 183–191.

38. Ling, C., Yamashita, M., Waselchuk, E.A., Raasch, J.L., Bless, D.M., and Welham, N.V. (2010). Alteration in cellular morphology, density and distribution in rat vocal fold mucosa following injury. Wound Repair Regen. 18, 89–97.

39. Paul, B.C., Rafii, B.Y., Gandonu, S., Bing, R., Born, H., Amin, M.R., and Branski, R.C. (2014). Smad3: an emerging target for vocal fold fibrosis. Laryngoscope 124, 2327–2331.

40. Neuman, R.E., and Logan, M.A. (1950). The determination of hydroxyproline. J. Biol. Chem. 184, 299–306.

41. Ford, C.N., Roy, N., Sandage, M., and Bless, D.M. (1998). Rigid endoscopy for monitoring indirect vocal fold injection. Laryngoscope 108, 1584–1586.

42. Inagi, K., Connor, N.P., Ford, C.N., Schultz, E., Rodriquez, A.A., Bless, D.M., Pasic, T., and Heisey, D.M. (1998). Physiologic assessment of botulinum toxin effects in the rat larynx. Laryngoscope 108, 1048–1054.

43. Kawasaki, K., Ushioda, R., Ito, S., Ikeda, K., Masago, Y., and Nagata, K. (2015). Deletion of the collagen-specific molecular chaperone Hsp47 causes endoplasmic reticulum stress-mediated apoptosis of hepatic stellate cells. J. Biol. Chem. 290, 3639–3646.

44. Kendziorski, C.M., Newton, M.A., Lan, H., and Gould, M.N. (2003). On parametric empirical Bayes methods for comparing multiple groups using replicated gene expression profiles. Stat. Med. 22, 3899–3914.

45. Kuleshov, M.V., Jones, M.R., Rouillard, A.D., Fernandez, N.F., Duan, Q., Wang, Z., Koplev, S., Jenkins, S.L., Jagodnik, K.M., Lachmann, A., et al. (2016). Enrichr: a comprehensive gene set enrichment analysis web server 2016 update. Nucleic Acids Res. 44 (W1), W90-7.

46. Chen, E.Y., Tan, C.M., Kou, Y., Duan, Q., Wang, Z., Meirelles, G.V., Clark, N.R., and Ma'ayan, A. (2013). Enrichr: interactive and collaborative HTML5 gene list enrichment analysis tool. BMC Bioinformatics 14, 128.

47. Blake, J.A., Dolan, M., Drabkin, H., Hill, D.P., Li, N., Sitnikov, D., Bridges, S., Burgess, S., Buza, T., McCarthy, F., et al.; Gene Ontology Consortium (2013). Gene Ontology annotations and resources. Nucleic Acids Res. *41*, D530–D535.

48. Wingstrand, V.L., Grønhøj Larsen, C., Jensen, D.H., Bork, K., Sebbesen, L., Balle, J., Fischer-Nielsen, A., and von Buchwald, C. (2016). Mesenchymal stem cell therapy for the treatment of vocal fold scarring: a systematic review of preclinical studies. PLoS ONE *11*, e0162349.

49. Bless, D.M., and Welham, N.V. (2010). Characterization of vocal fold scar formation, prophylaxis, and treatment using animal models. Curr. Opin. Otolaryngol. Head Neck Surg. *18*, 481–486.

50. Hiwatashi, N., Kraja, I., Benedict, P.A., Dion, G.R., Bing, R., Rousseau, B., Amin, M.R., Nalband, D.M., Kirshenbaum, K., and Branski, R.C. (2018). Nanoparticle delivery of RNA-based therapeutics to alter the vocal fold tissue response to injury. Laryngoscope *128*, E178–E183.

51. Chang, Z., Kishimoto, Y., Hasan, A., and Welham, N.V. (2014). TGF-β3 modulates the inflammatory environment and reduces scar formation following vocal fold mucosal injury in rats. Dis. Model. Mech. *7*, 83–91.

52. Hall, J.E., Suehiro, A., Branski, R.C., Garrett, C.G., and Rousseau, B. (2012). Modulation of inflammatory and profibrotic signaling in a rabbit model of acute phonotrauma using triamcinolone. Otolaryngol. Head Neck Surg. *147*, 302–307.

53. Pucci, B., Kasten, M., and Giordano, A. (2000). Cell cycle and apoptosis. Neoplasia *2*, 291–299.

54. Kim, D.-H., Behlke, M.A., Rose, S.D., Chang, M.-S., Choi, S., and Rossi, J.J. (2005). Synthetic dsRNA Dicer substrates enhance RNAi potency and efficacy. Nat. Biotechnol. *23*, 222–226.

55. Kim, D.-H., Longo, M., Han, Y., Lundberg, P., Cantin, E., and Rossi, J.J. (2004). Interferon induction by siRNAs and ssRNAs synthesized by phage polymerase. Nat. Biotechnol. *22*, 321–325.

56. Gugatschka, M., Ainödhofer, H., Gruber, H.J., Graupp, M., Kieslinger, P., Kiesler, K., Saxena, A., Hirano, S., and Friedrich, G. (2014). Age effects on extracellular matrix production of vocal fold scar fibroblasts in rats. Eur. Arch. Otorhinolaryngol. *271*, 1107–1112.

57. Graupp, M., Kiesler, K., Friedrich, G., Ainödhofer, H., Gruber, H.-J., Kieslinger, P., Saxena, A., Hirano, S., and Gugatschka, M. (2014). Vocal fold fibroblast response to growth factor treatment is age dependent: results from an in vitro study. J. Voice *28*, 420–423.

58. Gray, S.D., Titze, I.R., Alipour, F., and Hammond, T.H. (2000). Biomechanical and histologic observations of vocal fold fibrous proteins. Ann. Otol. Rhinol. Laryngol. *109*, 77–85.

59. Gray, S.D., Titze, I.R., Chan, R., and Hammond, T.H. (1999). Vocal fold proteoglycans and their influence on biomechanics. Laryngoscope *109*, 845–854.

60. Toya, Y., Riabroy, N., Davis, C.R., Kishimoto, Y., Tanumihardjo, S.A., Bless, D.M., and Welham, N.V. (2014). Interspecies comparison of stellate cell-containing macula flavae and vitamin A storage in vocal fold mucosa. J. Anat. *225*, 298–305.

61. Ling, C., Yamashita, M., Zhang, J., Bless, D.M., and Welham, N.V. (2010). Reactive response of fibrocytes to vocal fold mucosal injury in rat. Wound Repair Regen. *18*, 514–523.

62. Tateya, I., Tateya, T., Lim, X., Sohn, J.H., and Bless, D.M. (2006). Cell production in injured vocal folds: a rat study. Ann. Otol. Rhinol. Laryngol. *115*, 135–143.

63. Obata, Y., Nishino, T., Kushibiki, T., Tomoshige, R., Xia, Z., Miyazaki, M., Abe, K., Koji, T., Tabata, Y., and Kohno, S. (2012). HSP47 siRNA conjugated with cationized gelatin microspheres suppresses peritoneal fibrosis in mice. Acta Biomater. *8*, 2688–2696.

64. Livak, K.J., and Schmittgen, T.D. (2001). Analysis of relative gene expression data using real-time quantitative PCR and the $2^{-\Delta\Delta CT}$ Method. Methods *25*, 402–408.

65. Chang, Z., Ling, C., Yamashita, M., and Welham, N.V. (2010). Microarray-driven validation of reference genes for quantitative real-time polymerase chain reaction in a rat vocal fold model of mucosal injury. Anal. Biochem. *406*, 214–221.

66. R Development Core Team (2007). R: a language and environment for statistical computing (Vienna: R Foundation for Statistical Computing).

67. Irizarry, R.A., Hobbs, B., Collin, F., Beazer-Barclay, Y.D., Antonellis, K.J., Scherf, U., and Speed, T.P. (2003). Exploration, normalization, and summaries of high density oligonucleotide array probe level data. Biostatistics *4*, 249–264.

68. Wu, Z., and Irizarry, R.A. (2004). Preprocessing of oligonucleotide array data. Nat. Biotechnol. *22*, 656–658, author reply 658.

69. Supek, F., Bošnjak, M., Škunca, N., and Šmuc, T. (2011). REVIGO summarizes and visualizes long lists of gene ontology terms. PLoS ONE *6*, e21800.

70. Cline, M.S., Smoot, M., Cerami, E., Kuchinsky, A., Landys, N., Workman, C., Christmas, R., Avila-Campilo, I., Creech, M., Gross, B., et al. (2007). Integration of biological networks and gene expression data using Cytoscape. Nat. Protoc. *2*, 2366–2382.